

Optic Disc and Cup Segmentation for Glaucoma Characterization Using Deep Learning

Jongwoo Kim
Lister Hill National Center for
Biomedical Communications
National Library of Medicine
National Institutes of Health
Bethesda, USA
jongkim@mail.nih.gov

Loc Tran
Lister Hill National Center for
Biomedical Communications
National Library of Medicine
National Institutes of Health
Bethesda, USA
lotran@mail.nih.gov

Emily Y. Chew
Division of Epidemiology &
Clinical Applications
National Eye Institute
National Institutes of Health
Bethesda, USA
echew@nei.nih.gov

Sameer Antani
Lister Hill National Center for
Biomedical Communications
National Library of Medicine
National Institutes of Health
Bethesda, USA
santani@mail.nih.gov

Abstract—Glaucoma is one of the most common eye diseases that can cause irreversible vision loss due to damage to the optic nerve. Ophthalmologists consider a cup to optic disc ratio greater than 0.3 to be suggestive of glaucoma. Unfortunately, there is high variability among ophthalmologists in estimating the ratio since it is not easy to reliably measure optic disc and cup areas in a fundus image. Therefore, this paper proposes automatic methods to segment the optic disc and cup areas. There are two steps to estimate the ratio: region of interest (ROI) area detection (where optic disc is in the center) from a fundus image, followed by optic disc and cup segmentation. This paper focuses on automated methods to segment the optic disc and cup from the ROI. Fully convolutional networks (FCN) with U-Net architectures are used for the segmentation. The RIGA dataset (composed of three different fundus image datasets: MESSIDOR, Bin Rushed, and Magrabi), containing 750 fundus images, is used to train and test the FCNs. Our proposed FCNs show relatively better performance than other existing algorithms. The best segmentation results for optic disc show 0.95 Jaccard index, 0.98 F-measure, and 0.99 accuracy. The best segmentation results for cup show 0.80 Jaccard index, 0.88 F-measure, and 0.99 accuracy.

Keywords— Glaucoma, Region of Interest (ROI), Optic Disc, Cup, Deep Learning, Fully Convolutional Neural Networks (FCN), U-Net

I. INTRODUCTION

Glaucoma is a group of diseases that can damage the optic nerve. There are often no symptoms in its early stages. It can lead to vision loss and blindness if it is left untreated [1]. It is the second leading cause of blindness in the world and about 80 million people will suffer from the disease by 2020 [2]. In USA, 2.7 million people suffer from glaucoma and the patients will increase to 4.2 million by 2030. African Americans above age 40, and anyone age above 60 have higher risk of glaucoma. Therefore, a comprehensive dilated eye exam every 1-2 years is necessary for early detection of the disease [3].

In a fundus image, optic disc is the area where blood vessels and optic nerve fibers enter the retina and cup is the bright area in the center of optic disc where no nerve fibers exist. In most types of glaucoma, high intraocular pressure damages the optic nerve. This causes the cup to become larger in comparison to the optic disc. A cup to optic disc ratio greater than 0.3 is considered to be suspicious for glaucoma [1]. Unfortunately, it is not easy to measure optic disc and cup areas for ophthalmologists. Ophthalmologists often disagree on

segmentation results of each other [4]. It also takes minutes per eye to segment optic disc and cup [5].

There are several approaches to segment optic disc and cup from fundus images for glaucoma. Since blood vessels are emanating from the cup, they are used for optic disc segmentation [6, 7, 8, 9]. Thresholding methods are used to estimate optic disc candidate areas [6], and blood vessels and features extracted from the candidate areas are used to estimate the optic disc [7, 9]. Ellipse fitting methods are commonly used to estimate the final optic disc area [7, 8, 9, 10]. The performances in these methods depend heavily on good binarization algorithms. Deep learning is recently adapted in image enhancement [12] and image segmentation [12, 13, 14]. Among the FCNs, U-Net architecture [14] is the most commonly used to segment images. Different deep learning architectures are also used to segment optic disc and cup [15, 16] recently. We use a FCN to segment optic disc in our preliminary work [17]. Therefore, in this paper, we further expand our work and propose new algorithms to segment optic disc and cup using FCNs with U-Net architecture. We evaluate two different FCNs: one for binary output and the other for multi-class output. We also use two different input images to segment the cup. One is the original image and the other is the image masked by optic disc.

The remainder of this paper is organized as follows. Section II describes data that we use. Section III describes our methods to segment optic disc and cup in detail. We discuss experimental results and discussion in Section VI, and conclude in Section V.

II. DATA

We use the RIGA dataset, a publicly available fundus image dataset from University of Michigan [4]. The dataset is composed of three subsets. MESSIDOR, Bin Rushed, and Magrabi. Each data set contains fundus images and their corresponding annotations of optic disc and cup by six ophthalmologists. MESSIDOR contains 460 images, Magrabi contains 94 images, and Bin Rushed contains 195 images. However, 50 Bin Rushed images do not contain fundus images (images without any optic disc and cup annotations). Therefore, we use 145 images from Bin Rushed. In total, we use 699 images in the experiments. The image sizes are 2160×1440. To collect ROI images from the dataset, we crop a square area (in each

This research was supported by the Intramural Research Program of the National Institutes of Health, National Library of Medicine, and Lister Hill National Center for Biomedical Communications.

image) that has width and height two times the largest optic disc diameter in the image.

Each fundus image has six optic disc and cup annotations done by six ophthalmologists [4]. Unfortunately, high subjectivity has been noted among ophthalmologists in the annotations. The annotations of each ophthalmologist are evaluated by five other ophthalmologists. The average inter-reader agreements of these peer-to-peer reviews of optic disc and cup annotations are 0.643 and 0.633 respectively. The best inter-reader agreement for optic disc measurement ranges between 0.647 and 0.745. The best inter-reader agreement for cup measurement ranges between 0.538 and 0.724. It shows that the optic disc and cup segmentation is a very challenging issue, even for ophthalmologists. It is hard choosing ground-truth data for optic disc and cup among the results of the six ophthalmologists. In our case, we choose the results of an ophthalmologist who has the best agreement in optic disc and the results of another ophthalmologist who has the best agreement in cup for the ground-truth data.

III. METHODS

There are two steps to estimate optic disc and cup area in our method. First, region of interest detection (ROI) from fundus images where the optic disc is in the center. Second, optic disc and cup segmentation from the ROI. We will focus on the segmentation in the second step in this paper. There are several ways for the second step: segmentation of optic disc from the ROI, segmentation of cup from the ROI, segmentation of cup from optic disc, and segmentation of optic disc and cup from the ROI simultaneously. We will train the FCNs for each case and evaluate their performance later.

A. Region of Interest (ROI) Detection

A conventional convolutional neural network (CNN) is used to detect the ROI area [18]. The CNN is composed of two convolutional layers, two max pooling layers, two fully connected layers, and one output layer. We use the following steps for the ROI detection. First, train the CNN using ROI and Non-ROI class images cropped from the training fundus image set. Second, estimate an ellipse in an input fundus image that fits to the edge of the retina using Otsu threshold. Third, set the window size W = longest diameter of the ellipse/3.5 and stride $S = W/4$. Fourth, move $W \times W$ window to the horizontal and vertical directions by S in the fundus image, estimate the CNN result of each window, and choose a window W_1 that has the highest CNN result as the ROI of the fundus image. Fig. 1 shows examples of the estimation results. Green boxes in the images show the estimated ROIs.

B. Fully Convolutional Networks (FCNs)

As shown in Fig. 2, we use FCNs with U-Net structures implemented by using Python and Tensorflow with Keras [19, 20] for the segment of the optic disc and cup from the ROI images. Input of the FCN is $224 \times 224 \times 3$ color images and output is $224 \times 224 \times 1$ binary or grey level images depending on the number of label classes. The FCNs are composed of two paths: Contraction path and expansive path. The contracting path (left side) consists of convolutional layers and max pooling layers. The expansive path (right side) consists of upsampling

of the feature map and convolutional layers. Two dropout layers are added in the contracting path to train the FCNs more robustly. The final convolutional layer maps each feature vector to the desired classes. The FCNs assign a class label to each pixel as an output.

We use two different FCNs: FCN2 (a U-Net architecture for two-class segmentation) and FCNM (a U-Net architecture for multi-class segmentation). The FCN2 is used in most of our two-class segmentation experiments and the FCNM is used to segment the optic disc and cup simultaneously.

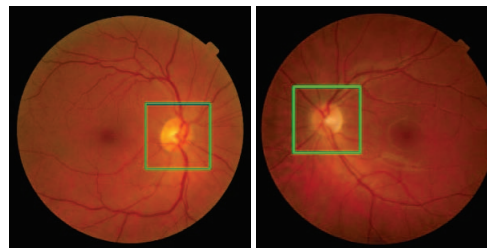


Figure 1. ROIs (Green boxes) detected by using the CNN.

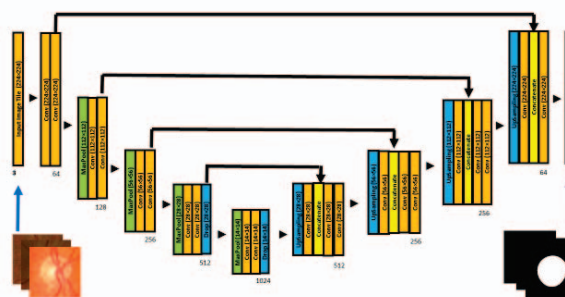


Figure 2. Architecture of the FCN used in this experiment.

IV. RESULTS AND DISCUSSION

In this section, we present the experimental results in detail.

A. Training FCNs

It is relatively easy to identify the optic disc in a fundus image because it has high intensity pixel values and has a circular/oval shape. However, it is more challenging work to estimate cup from optic disc even if cup has higher pixel values than optic disc. Therefore, we train FCNs three different ways to segment optic disc and cup. First, train a FCN2 to estimate optic from ROI and train another FCN2 to estimate cup from a ROI. Second, train a FCNM to segment optic disc and cup from a ROI simultaneously. Third, train a FCN2 to segment optic disc from a ROI and train another FCN2 to segment cup from a ROI masked by optic disc (called the masked ROI).

From the RIGA dataset, we collect 699 ROIs to train and test by cropping the fundus images in the dataset. The width and height of the cropped image are two times the largest optic disc diameter. We then normalize the images to 224×224 for training the FCNs. We perform five-fold cross-validation to estimate the segmentation results since the dataset is small relative to dataset

sizes typically used for deep learning. We use a maximum of 500 epochs, batch size = 20, Adam optimization algorithm (learning rate = 1e-5, first beta = 0.9, second beta = 0.999, epsilon = 1e-07, and decay=0.0) for training, and save the best results as output of the training results during the training time. We use NVIDIA GeForce GTX1080-Ti for training.

Fig. 3 shows some images used for training and testing. The first column is an image from Bin Rushed, the second column is from MESSIDOR, and the third column is from Magrabi. The first row shows ROIs from fundus images, the second row shows the ground-truth cup images, the third row shows the ground-truth optic disc images, and the last row shows the ground-truth of combined optic disc and cup images. FCN2 uses the images in the second or third rows as output for training and FCNM uses the images in the fourth row for training. Fig. 4 shows examples of the masked ROIs. The masked ROIs are created by overlapping the original ROIs with the corresponding optic disc images.

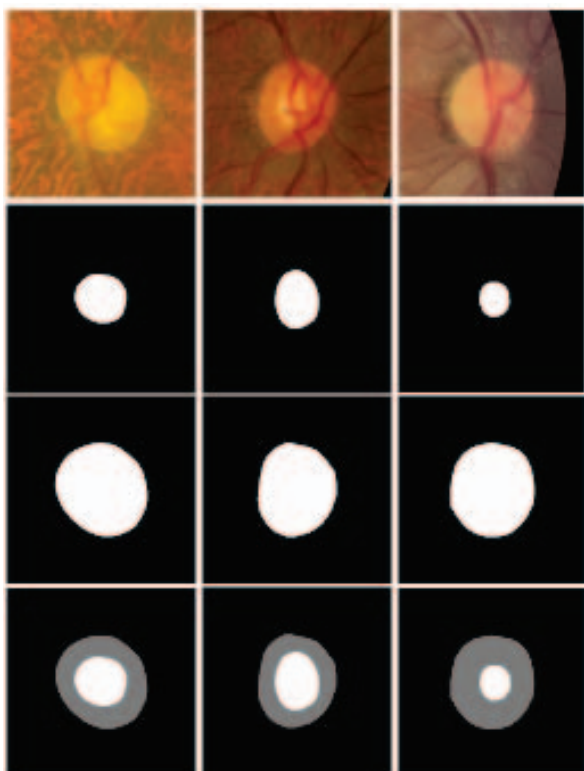


Figure 3. ROIs and their corresponding ground truth optic disc and cup images. The first row is ROI, the second row is cup, the third row is optic disc, and the last row is optic disc and cup images.

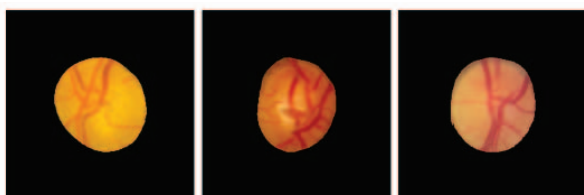


Figure 4. Example of ROIs masked by optic discs (masked ROIs).

To reduce the intensity variation among images in our data, we normalize the images using the mean and standard deviation of each image before training the FCN as shown in Equation (1).

$$I_N(i, j, k) = \frac{I(i, j, k) - m_k}{\sigma_k} \quad (1)$$

In the equation, $I(i, j, k)$ is an input image, $I_N(i, j, k)$ is a normalized pixel value of $I(i, j, k)$, i and j are coordinates of the images I and I_N , $k = \text{Blue, Green, or Red channel}$, m_k is the mean of pixel values of channel k , and σ_k is standard deviation of pixel values of channel k .

Due to a limited number of ROIs for training the FCNs, we augment the ROIs to increase their number for training the FCNs. We use one flip and five different rotations $[0, 15, 30, 330, 345]$ to augment the training images.

Fig. 5 shows the diagram and parameters used to evaluate our performance. The green region (G) is the ground truth and the blue region (E) is our estimated result. TP stands for true positive, TN for true negative, FN for false negative, and FP for false positive. Based on the parameters in the diagram, we use eight metrics to evaluate our performance and some of the metrics are shown in the equations (2)–(7).

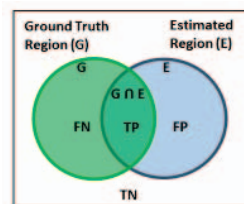


Figure 5. Diagram used to evaluate the performance

$$\text{Jaccard Index} = \frac{G \cap E}{G \cup E} = \frac{TP}{TP + FP + FN} \quad (2)$$

$$F - \text{Measure} (F - \text{Mea}) = \frac{2 \times TP}{2 \times TP + FP + FN} \quad (3)$$

$$\text{Accuracy} (ACC) = \frac{TP + TN}{TP + TN + FP + FN} \quad (4)$$

$$\text{Sensitivity} (SEN) = \frac{TP}{TP + FN} \quad (5)$$

$$\text{Specificity} (SPE) = \frac{TN}{TN + FP} \quad (6)$$

$$\text{Mean of Sen and Spec} (MSS) = \frac{SEN + SPE}{2} \quad (7)$$

B. Optic Disc Segmentation

Table I shows the test results of optic disc segmentation. We train two different FCNs. FCN2 uses ROIs (the first row in Fig. 3) as inputs and optic disc images (the third row in Fig. 3) as outputs to train the model. FCNM uses the same ROIs as inputs and optic disc and cup images (the fourth row in Fig. 3) as output, and generates independent optic disc and cup results (like images in the second and third rows in Fig. 3) from the output to evaluate the results. As shown in the table, the FCN2 (second column) shows better performance than FCNM (third column) in all metrics. Table II shows analysis of the FCN2 results for each dataset of the first fold of the cross-validation. All datasets have relatively good results.

TABLE I. COMPARISON OF OPTIC DISC SEGMENTATION RESULTS

FCN Model	FCN2	FCNM
Input Image	ROI	ROI
Jaccard Index	0.9430	0.9381
Sensitivity	0.9798	0.9763
Specificity	0.9910	0.9906
MSS	0.9854	0.9834
Precision	0.9620	0.9603
Recall	0.9798	0.9763
F-Measure	0.9702	0.9674
Accuracy	0.9889	0.9879

TABLE II. COMPARISON OF OPTIC DISC SEGMENTATION RESULTS FROM FCN2 (SECOND COLUMN IN TABLE I) FOR EACH DATASET

FCN2	MESSIDOR	Magrabi	Bin-Rushed
Input Image	92	20	31
Jaccard Index	0.9527	0.9495	0.9478
Sensitivity	0.9770	0.9852	0.9653
Specificity	0.9944	0.9920	0.9959
MSS	0.9857	0.9886	0.9806
Precision	0.9749	0.9636	0.9816
Recall	0.9770	0.9852	0.9653
F-Measure	0.9757	0.9741	0.9730
Accuracy	0.9912	0.9907	0.9902

C. Cup Segmentation

Table III shows the results of cup segmentation. We use two different FCNs and three different tests to segment cup. The FCN2 in the second column uses ROIs as inputs and cup images (the second row in Fig. 3) as outputs to train the FCN. FCNM in the third column uses the ROIs as inputs and optic disc and cup images (the fourth row in Fig. 3) as output, and generate independent optic disc and cup results from the output to evaluate the results. The FCN2 in the fourth columns uses ROIs masked by optic discs (masked ROIs) as inputs as shown in Fig. 4. Boundary of optic disc from retina is relatively clear. However, boundary of cup from optic disc is ambiguous. Therefore, to let the FCN2 more focus on segmenting cup from optic disc, we use the masked ROIs as inputs. As shown in the table, the FCN2 using the masked ROI images (fourth column) shows the best performance in Jaccard index, specificity, precision, F-measure, and accuracy. The FCNM using original ROIs (third column) shows the best performance in sensitivity, MSS, and recall. Table IV shows analysis of the FCN2 results of the fourth column in Table III for each dataset of the first fold of the cross-validation. The result of MESSIDOR shows better results in Jaccard index, specificity, precision, F-measure, and accuracy, and the result of Bin-Rushed shows better results in sensitivity, MSS, and Recall.

Among the 8 performance metrics in the tables, some metrics use TN. The larger the ROI size is, the more TN pixels there are (large size ROI includes more pixels not belongs to optic disc). Since most TN pixels (pixels not belonging to optic disc) are easily classified, large ROI size inflates performance as given by some metrics, such as MSS and accuracy. Among the other remaining metrics, only Jaccard index uses TP, FP, and FN. Therefore, we use Jaccard index as a main metric to measure the performance of the FCNs. We choose the FCN2 (Second column) in Table I as the best FCN for optic disc segmentation and the FCN2 (fourth column) in Table III as the best FCN for cup segmentation.

TABLE III. ACCURACY OF CUP SEGMENTATION

FCN Model	FCN2	FCNM	FCN2
Input Image	ROI	ROI	Masked ROI
Jaccard Index	0.7921	0.7809	0.8037
Sensitivity	0.9362	0.9424	0.9265
Specificity	0.9905	0.9892	0.9924
MSS	0.9634	0.9658	0.9594
Precision	0.8459	0.8296	0.8674
Recall	0.9362	0.9424	0.9265
F-Measure	0.8789	0.8715	0.8873
Accuracy	0.9871	0.9861	0.9882

TABLE IV. COMPARISON OF CUP SEGMENTATION RESULTS FROM FCN2 (FOURTH COLUMN IN TABLE III) FOR EACH DATASET

FCN2	MESSIDOR	Magrabi	Bin-Rushed
Input Image	92	20	31
Jaccard Index	0.8327	0.7392	0.7193
Sensitivity	0.9120	0.9341	0.9442
Specificity	0.9948	0.9893	0.9877
MSS	0.9534	0.9617	0.9660
Precision	0.9123	0.7937	0.7642
Recall	0.9120	0.9341	0.9442
F-Measure	0.9066	0.8416	0.8301
Accuracy	0.9895	0.9862	0.9850

Fig. 6 shows optic disc segmentation results of the proposed FCNs. The images in the first row are from FCN2 and the images in the second row are from FCNM. In the figures, green represents ground-truth boundary and blue represents our estimated results. Both rows show good estimation results and the results of FCN2 (first row) show slightly better than the results of FCNM (second row). Fig. 7 shows cup segmentation results of the proposed FCNs. The images in the first column are from FCN2 using the original ROIs (second column in Table III), the images in the second column are from FCNM using the ROIs (third column in Table III), and the images in the last column are from FCN2 using the masked ROIs (fourth column in Table III). In the figures, green represents ground-

truth boundary and blue represents our estimated results. All columns show good estimation results. However, the results of FCN2 using the masked ROIs in the third column show slightly better than other results.

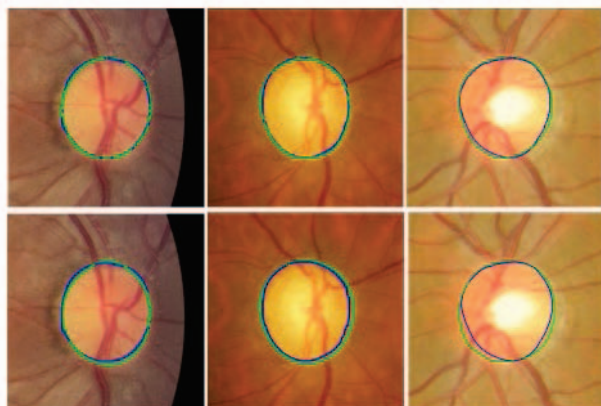


Figure 6. Optic disc segmentation results of the proposed FCNs. First row is from FCN2 and the second row is from FCNM.

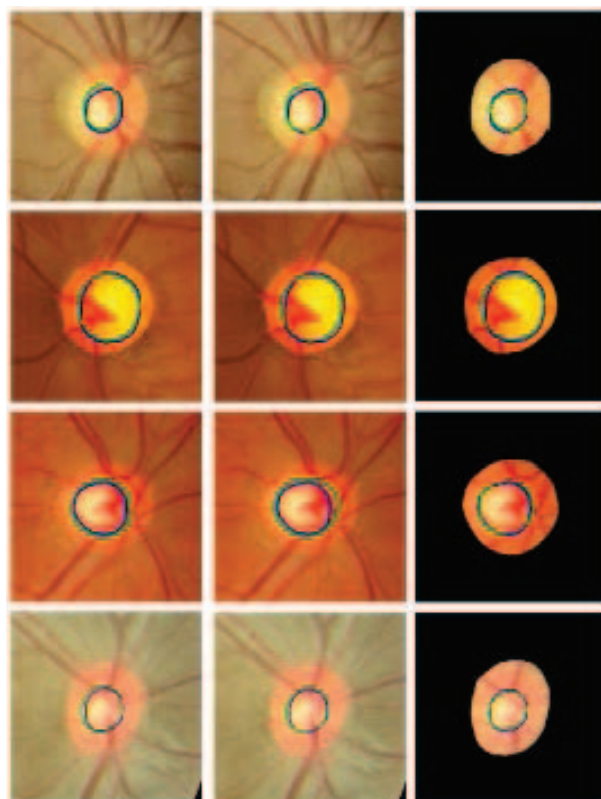


Figure 7. Cup segmentation results of the proposed FCNs. The first column is from FCN2, the second column is from FCNM. The last column is from FCN2 using the masked ROI.

While we compare our results with other algorithms, as shown in Table V and VI, it should be noted that they are using different datasets and ROI sizes. Larger size ROIs usually have more TN pixels (pixels farther from optic disc) and the pixels are relatively easy to classify correctly. Therefore, among the metrics, MSS, specificity, and accuracy have better performance score when ROIs have more TN pixels. All other metrics such as Jaccard index, f-measure, etc. do not use TN in their formulas.

Table V shows comparison of our optic disc segmentation results with others. The proposed FCN2 (second column in Table I) shows the best results in Jaccard index, MSS, and f-measure. Al-Bander’s algorithm shows the best results in accuracy. Table VI shows the comparison of our cup segmentation results with others. The proposed FCN2 using the masked ROI (fourth column in Table III) shows the best performance in Jaccard index, MSS, and f-measure. The Al-Bander’s algorithm shows the best performance in accuracy. As shown in the two tables, our algorithms show relatively good performance in all metrics especially in Jaccard index that considers areas of ground-truth and estimated output of our interest area (optic disc or cup area), not the TN areas.

TABLE V. COMPARISON OF OUR OPTIC DISC SEGMENTATION RESULTS WITH OTHER ALGORITHMS

Method	Cheng [7]	Al-Bander [15]	Fu [16]	Proposed FCN2
Jaccard Index	0.8980	0.9311	0.9290	0.9430
MSS	0.9640	0.9845	0.9830	0.9854
F-Measure	-	0.9640	-	0.9702
Accuracy	-	0.9989	-	0.9889
Database	MESSIDOR	ORIGA	ORIGA	RIGA: MESSIDO R, Bin Rushed, Magrabi

TABLE VI. COMPARISON OF OUR CUP SEGMENTATION RESULTS WITH OTHER ALGORITHMS

Method	Cheng [7]	Al-Bander [15]	Fu [16]	Proposed FCN2
Jaccard Index	0.7360	0.7788	0.7300	0.8037
MSS	0.9180	0.9381	0.9300	0.9594
F-Measure	-	0.8723	-	0.8873
Accuracy	-	0.9986	-	0.9882
Database	MESSIDOR	ORIGA	ORIGA	RIGA: MESSIDO R, Bin Rushed, Magrabi

V. CONCLUSIONS

This paper proposes automatic methods to segment optic disc and cup from ROIs in fundus images to estimate optic disc to cup ratio for glaucoma. We implement two different (binary and multi-class) FCNs and try two different ROIs (original ROI and masked ROI) as inputs to estimate the best segmentation results. The segmentation results of the proposed FCNs are promising. The FCN for optic disc segmentation shows better performance than other existing algorithms in Jaccard index, ACC, and f-measure. The FCN for cup segmentation also shows better performance in Jaccard index, ACC, and f-measure. The FCNs for binary class show better performance than the FCNs for multi-class. As future work, we plan to use more complex FCN structures such as GAN and Mask-RCNN to improve segmentation accuracy.

ACKNOWLEDGMENT

This research was supported by the Intramural Research Program of the National Institutes of Health, National Library of Medicine, and Lister Hill National Center for Biomedical Communications. We thank Dr. Ahmed Almazroa from the University of Michigan for providing the RIGA dataset. In addition, we acknowledge the help of the National Eye Institute staff in providing additional fundus images (AREDS dataset) to extend the current work.

REFERENCES

- [1] Glaucoma Research Foundation, <https://www.glaucoma.org/>.
- [2] H.A. Quigley and A.T. Broman, "The number of people with glaucoma worldwide in 2010 and 2020," *Th british Journal of Ophthalmology*, Vol 90, no. 3, pp. 262-267, 2006
- [3] <https://nei.nih.gov/eyedata>
- [4] A. Almazroa, S. Alodhayb, E. Osman, E. Ramadan, M. Hummadi, M. Dlaim, M. Alkatee, K. Raahemifar, V. Lakshminarayanan, "Agreement among ophthalmologists in marking the optic disc and optic cup in fundus images", *International Ophthalmology*, vol. 37, pp. 701-717, 2017.
- [5] C. Lim, Y Cheng, W. Hsu, and M. L. Lee, "Integrated Optic Disc and Cup Segmentation with Deep Learning," *IEEE 27th International Conference on Tools with Artificial Intelligence*, vol. 19, no 3, pp. 162-169, November 2015.
- [6] A. Almazroa, S. Alodhayb, K. Raahemifar, V. Lakshminarayanan, "Optic Cup Segmentation: Type-II Fuzzy Thresholding Approach and Blood Vessel Extraction", *Clinical Ophthalmology*, vol. 11, pp. 841-854, 2017.
- [7] S. Roychowdhury, D. D. Koozekanani, S. N. Kuchinka, and K. K. Parhi, "Optic Disc Boundary and Vessel Origin Segmentation of Fundus Images," *IEEE Journal of Biomedical and Health Informatics*, vol. 20, no 6, pp. 1562-1574, November 2016.
- [8] D. Marin, M.E. Gegundez-Arias, A. Suero, and J. M. Bravo, "Obtaining optic disc center and pixel region by automatic thresholding methods on morphologically processed fundus images", *Computer Methods and Programs in Biomedicine*, pp. 173-185, 2015.
- [9] S. Morales, V. Naranjo, J. Angulo, and M. Alcaniz, "Automatic Detection of Optic Disc Based on PCA and Mathematical Morphology", *IEEE Transaction on Medical Imaging*, vol. 32, no. 4, pp. 369-376, April 2013.
- [10] J. Cheng, J Liu, Y Xu, F Yin, D.W.K. Wong, N. Tan, D. Tao, C. Cheng, T. Aung, T.Y. Wong, "Subpixel Classification Based on Optic Disc and Optic Cup Segmentation for Glaucoma Screening", *IEEE Trans Med Imaging*, Vol. 32, no 6, pp. 1019-1032, 2013.
- [11] S. Yu, D. Xiao, Y. Kanagasigam, "Machine Learning Based Automatic Neovascularization Detection on Optic Disc Region", *Journal of Biomedical and Health Informatics*, vol. 22 issue 3, 2018.
- [12] B. Savelli, A. Bria, A. Galdran, C. Marrocco, and M. Molinara, "Illumination correction by dehazing for retinal vessel segmentation" *IEEE 30th International Symposium on Computer-Based Medical Systems*, pp. 219-224, June 2017.
- [13] J. Son, S.J. Park, K. Jung, "Retina Vessel Segmentation in Fundoscopic Images with Generative Adversarial Networks", *DLMI 2017*, arXiv preprint, arXiv:1706.09318.
- [14] O. Ronneberger, P. Fischer, T. Brox, "U-Net: Convolutional Networks for Biomedical Image Segmentation", *Medical Image Computing and Computer-Assisted Intervention (MICCAI)*, Springer, LNCS, Vol.9351: 234--241, 2015.
- [15] B Al-Bander, B. M. Williams, W. Al-Nuaimy, M.A. Al-Tae, H. Pratt, and Y. Zheng, "Dense Fully Convolutional Segmentation of the Optic Disc and Cup in Colour Fundus for Glaucoma Diagnosis." *Symmetr*, Vol 10 Issue 4, 2018.
- [16] H. Fu, J. Cheng, Y. Xu, D.W.K. Wong, J. Liu, and X. Cao, "Joint Optic Disc and Cup Segmentation Based on Multi-Label Deep Network and Polar Transformation", *IEEE Transactions on Medical Imaging*, Vol 37, No, 7, July 2018
- [17] J. Kim, L. Tran, E. Chew, S. Antani, G.R. Thoma, "Optic Disc Segmentation Using Deep Learning", *SPIE Medical Imaging 2019*, accepted.
- [18] J. Kim, C. Candemir, E. Chew, G.R. Thoma, "Region of Interest Detection in Fundus Images Using Deep Learning and Blood Vessel Information", *The 31th IEEE International Symposium on Computer-Based Medical System*, pp. 357-362, June 2018.
- [19] <https://www.tensorflow.org/>
- [20] <https://keras.io/>